Heat transfer analysis in different cookware materials

J. Martínez, A. J. Riofrio, S. P. Villacis, J. P. Kastillo,
Instituto Nacional de Eficiencia Energética y Energías Renovables – INER.
Av. 6 de diciembre N33-32 e Ignacio Bossano Edificio Torre Bossano, 2do. Piso Quito, Ecuador
e-mail: javier.martinez@iner.gob.ec, javiermtnezg@gmail.com

Abstract— **Induction heating is a fast, efficient, precise and repeatable non-contact method for heating metals or other electrically-conductive materials. Induction cookers are domestically induction heating devices which have become more popular against gas based cookers and electrical resistance stoves because they are safer and they present higher heating rates and energy efficiency. However the appropriate performance of these devices for induction heating (IH) depends directly on the coupled system cooker-cookware. Differences in the energy efficiency and temperature distribution during heating and cooling are related to the configuration of the pot and the different materials which those are made of. In case of cooking processes, the natural convection of the different fluids may affect to the microbiology, safety, food quality and cooking times. This study aims to perform the heating analysis in the lateral of three different induction cookware configurations of aluminium, enameled iron and stainless steel body cookware. The experimental data was analyzed using COMSOL Multiphysics in order to understand the thermal processes in the different pots. These results were compared with the results obtained by a thermographic camera. Results show that pot materials have a direct influence in the heating rate and distribution.**

Keywords: Induction cookware, induction cooking, heat transfer analysis, pot, cast iron, thermography, COMSOL Multiphysics, Computational fluid dynamic.

I. INTRODUCTION

Induction heating is a non-contact heating process. It uses high frequency electricity to heat materials that are electrically conductive. Since it is non-contact, the heating process does not contaminate the material that is being heated. It is also very efficient since the heat is actually generated inside the cookware. This can be contrasted with other heating methods where heat is generated in a flame or in the heating element, which is then applied to the cookware [1]. This process has less energy losses, the material magnetically agitates, so the absorbed energy releases as energy, heating the cookware. For these reasons Induction Heating (IH) lends itself to some unique applications in industry. The IH technique has been developed since 1970 but they are recently becoming popular for heating food in households [1], [2], [3], [4], [5], [6], [7], [8].

The Government of Ecuador is looking forward to replace 3 million of liquefied petroleum based (LPG) based cookers for induction cookers, besides the introduction of cookware sets consisting of three pots with different diameters and a saucepan, being a world pioneer campaign called "efficient cooking plan", in order to achieve that, they have been working in several adaptation of the electrical grid and industry [9], [10].

A study of the heating process of the pots bottom in an induction cooker with a pot filled with water has been made. [8]. In this sense, this research aimed to perform a new analysis of the heating process in air in the sides of three types of pots, with different configurations, speaking about their body and bottom material, in order to know the temperature distribution, speed of heating and cooling, and the heat flux of pots during heating, in enameled cast iron, stainless steel and aluminium body with stainless steel bottom pots, in order to determine the most suitable pots for induction. A physical model has been studied using the multi analytic software COMSOL Multiphysics© and it has been validated with data obtained from a thermographic camera, through laboratory tests.

II. MATERIALS AND EXPERIMENTAL METHOD

A. Procedure

The procedure of the performed tests consists of pots heating without water, within laboratory conditions. The pots were located on an induction cooker, model Povos/Pentium C21-PH12T, it has only one induction zone with a nominal power of 1 000 W and a voltage of 110 V. The thermographic camera, model FLUKE Ti125 was used; it has a temperature scale from 60 °C to 385 °C. The thermographic camera was set perpendicular to the pot with a separation of 1,20 m as is shown in Figure. 1, this procedure was followed for the pot lateral. After that, the cooker was turned on while the thermographic camera was recording a video and saving in its memory the outstanding temperatures for this study. It was able to get the thermographies of the laterals at different instants of time and this has allowed getting the temperature distribution for several points of the laterals. It is important to notice that these tests were performed in the south of Quito, which is about 2800 meters above sea level, and has an atmospheric pressure of 728.4 hPa, which is the reason of the water boiling at 92 ° C

TABLE I. CHARACTERISTICS OF TESTED POTS

N°	Material of the body (BM)	Material of the bottom (BM)	Diameter of the bottom [cm]	Diameter of the top[cm]	Thickness of the body [mm]	Thickness of bottom [mm]	Thermal conductivity of BM $[\frac{W}{m \cdot K}]$	Density of BM $[\frac{g}{cm^3}]$	Specific heat of BM $[\frac{J}{kg \cdot K}]$	Mass [g]
1	Enameled iron	Enameled iron	17.00	20.00	0.7	1.0	53.3	7.18	500	468.00
2	AISI 304 Stainless steel	AISI 430 Stainless steel	17.00	20.00	0.5	1.8	24.9	7.80	505	900.50
3	Aluminium	AISI 430 Stainless steel	17.00	20.00	2	2.5	209	2.70	909	744.00

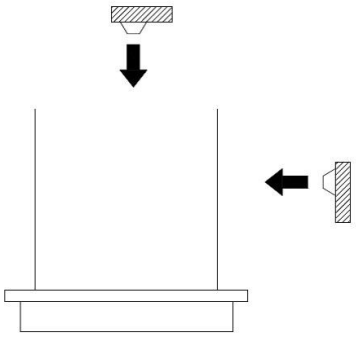

Figure. 1 Scheme of the procedure of recording measurements with the thermographic camera.

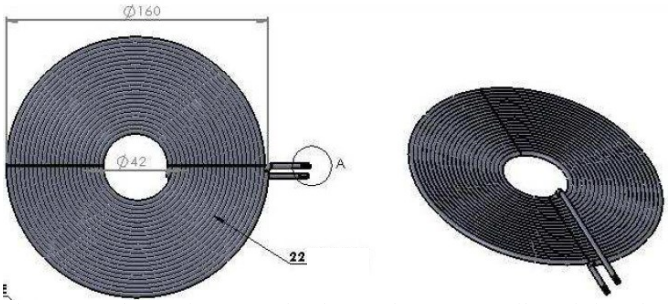

Figure 2 Scheme of Povos cooker from a plane cooper coil consisting of 22 wires of electrolytic copper and 0.5 mm of diameter.

TABLE I shows the main characteristics of the pots that were used in the tests, it has been chosen different material pots suitable for induction. The first configuration of cookware was tested in a pot made of enameled iron in its body and in its bottom; then the second cookware configuration was tested, it consists of pot made of AISI 304 stainless steel in its bottom and in its base a three layer material made of AISI 430 stainless steel, aluminium and iron, all of them weld together to its body and covered by an AISI 430 stainless steel layer. The last cookware configuration was tested, in a pot made of aluminium in its body and AISI 430 stainless Steel in its bottom.

The temperature analysis from the thermographic images during heating and cooling, central and extreme points were chosen. The values of temperatures were taken every five seconds; in the case of pots without water, measurements were taken until saturation temperature was reached, or until the temperature sensor of the cooker reaches its limit and it turns off.

Once that the heating test was performed, the cooker was turned off and the temperature during pot cooling was measured during ten minutes in the case of pots with water. The analyzed points were used to plot graphs of temperature against time.

The obtained temperature data was used to make a computational fluid dynamics (CFD) analysis, in order to get results related with convective heat flux, through the modulation and simulation with the software COMSOL Multiphysics©.

B. Assumptions

To simplify the problem, the following assumptions were made:

(1) Axi-symmetry: The shape of the pot was assumed to be a cylinder. The convection of fluid may show axial symmetry in the pot because the heating condition is axi-symmetrical.

(2) Heat generation due to viscous dissipation is negligible.

(3) Boussinesq approximation was applied for the buoyancy.

(4) The assumption of no-slip condition at the inside wall of the pot is valid.

(5) Convection in the pot was a laminar flow, because it was a natural convection.

(6) The gravity force of 9.8 m/s^2 was added axially in the pot.

The thermophysical properties of the oil were considered, temperature dependence, and their values change during CFD simulation.

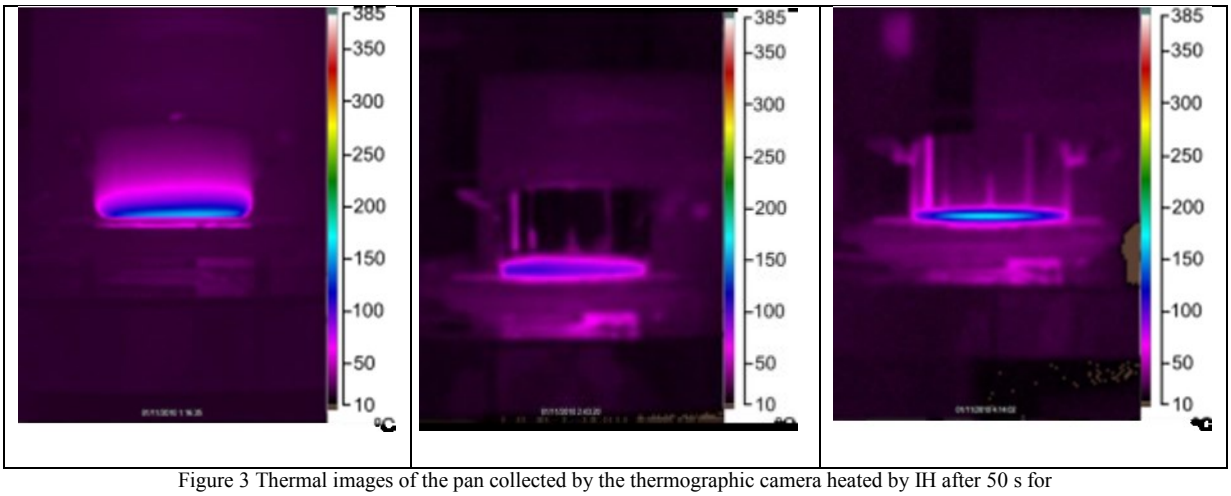

Figure 3 Thermal images of the pan collected by the thermographic camera heated by IH after 50 s for a) enameled iron, b) stainless steel and c) aluminium.

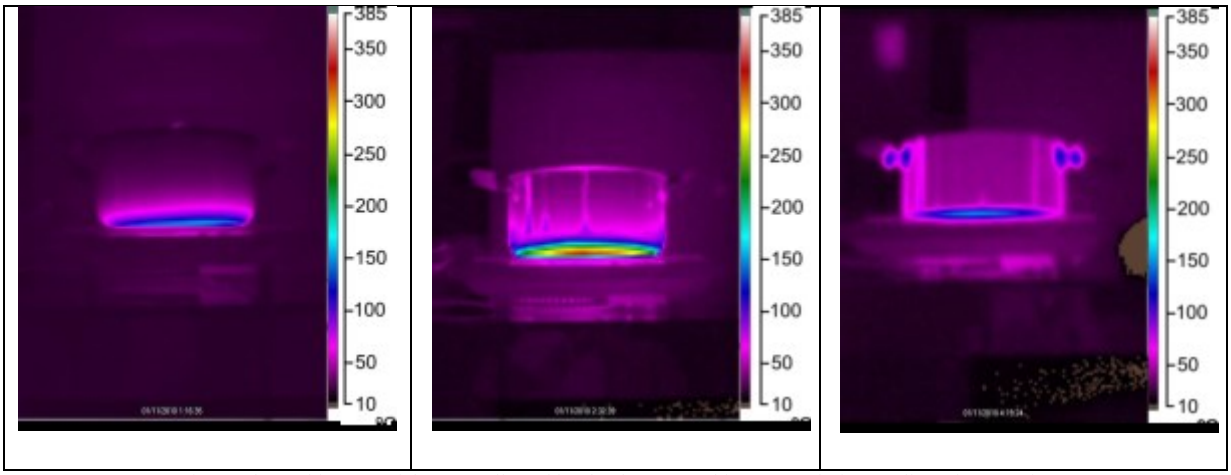

Fig. 4. Thermal images of the pan collected by the thermographic camera during cooling after 50 s for a) enameled iron, b) stainless steel and c) aluminium.

C. Model equations

The partial differential equations governing natural convection motion in a cylinder space are the Navier–Stokes equations in cylindrical coordinates [8] as you can find in:

(1) Continuity equation

$$\frac{1}{r}\frac{\partial}{\partial r}(rpv_r) + \frac{1}{r}\frac{\partial}{\partial \theta}(pv_\theta) + \frac{\partial}{\partial z}(pv_z) = 0 \qquad (1)$$

(2) Energy conservation equation

$$\frac{\partial T}{\partial t} + v_r\frac{\partial T}{\partial r} + \frac{v_\theta}{r}\frac{\partial T}{\partial \theta} + v_z\frac{\partial T}{\partial z} = \frac{k}{\rho C_p}\left[\frac{1}{r}\frac{\partial}{\partial r}\left(r\frac{\partial T}{\partial r}\right) + \frac{1}{r^2}\frac{\partial^2 T}{\partial \theta^2} + \frac{\partial^2 T}{\partial z^2}\right] \qquad (2)$$

In order to simplify the analysis, the buoyancy force caused by density variation with temperature was governed by the Boussinesq approximation shown in Eq. (3), which was used in the body force term of the momentum equation in the radial direction.

(3) Momentum equation

- In the radial direction (r)

$$r\left(\frac{\partial v_r}{\partial t} + v_r\frac{\partial v_r}{\partial r} + \frac{v_\theta}{r}\frac{\partial v_r}{\partial \theta} - \frac{v_\theta^2}{r} + v_z\frac{\partial v_r}{\partial z}\right) = -\frac{\partial p}{\partial r} + u\left[\frac{\partial}{\partial r}\left(\frac{1}{r}\frac{\partial}{\partial r}(rv_r)\right) + \frac{1}{r^2}\frac{\partial^2}{\partial \theta^2} - \frac{2}{r^2}\frac{\partial v_r}{\partial \theta} + \frac{\partial^2 v_r}{\partial z^2}\right] + \rho_{ref} g\left[1 - \beta(T - T_{ref})\right] \qquad (3)$$

where T_{ref} and ρ_{ref} are the reference temperature and density, respectively.

- In the vertical direction (z)

$$\rho\left(\frac{\partial v_z}{\partial t} + v_r\frac{\partial v_z}{\partial r} + \frac{v_\theta}{r}\frac{\partial v_z}{\partial \theta} + v_z\frac{\partial v_z}{\partial z}\right) = -\frac{\partial p}{\partial z} + \mu\left[\frac{1}{r}\frac{\partial}{\partial r}\left(r\frac{\partial v_z}{\partial r}\right) + \frac{1}{r^2}\frac{\partial^2 v_z}{v\theta^2} + \frac{\partial^2 v_z}{\partial z^2}\right] \qquad (4)$$

- In the angular direction (θ)

$$\rho\left(\frac{\partial v_\theta}{\partial t} + v_r\frac{\partial v_\theta}{\partial r} + \frac{v_\theta}{r}\frac{\partial v_\theta}{\partial \theta} + \frac{v_r v_\theta}{r} + v_z\frac{\partial v_\theta}{\partial z}\right) = -\frac{1}{r}\frac{\partial p}{\partial \theta} + \mu\left[\frac{\partial}{\partial r}\left(\frac{1}{r}\frac{\partial}{\partial r}(rv_\theta)\right) + \frac{1}{r^2}\frac{\partial^2 v_\theta}{\partial \theta^2} + \frac{2}{r^2}\frac{\partial v_r}{\partial \theta} + \frac{\partial^2 v_\theta}{\partial z^2}\right] \qquad (5)$$

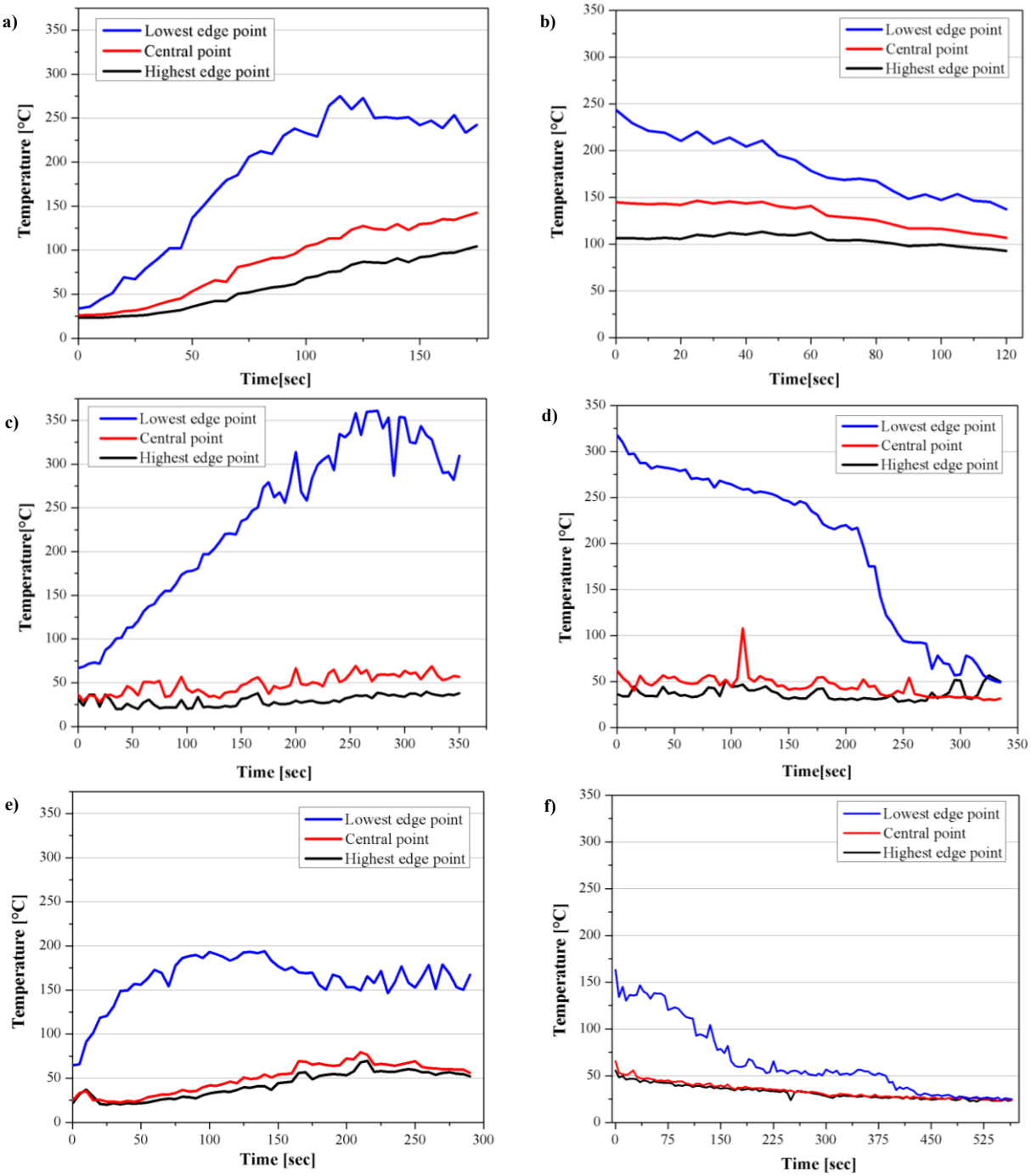

Fig. 5. Temperature distribution of the pan collected from the thermographic camera each 5 s for a) enameled iron, b) stainless steel and c) aluminium.

D. Solution strategy

The obtained temperature data was used to make a computational fluid dynamics (CFD) analysis, in order to get results related with convective heat flux, through the modulation and simulation with the software COMSOL Multiphysics©. Besides, this software was used to perform a performance analysis of cookware regarding the heat distribution.

II. RESULTS

A. Observation of heating location with termographic camera

Thermal images of the pan collected by the thermographic camera heated by IH after 50 s are shown in in Figure 3 a), b) and c) for enameled iron, stainless steel, and aluminium respectively.

The temperature on the sides of the pan was kept in low. Enameled iron increases its temperature in the base faster than stainless steel, and aluminium.

Thermal images of the pan collected by the thermographic camera during cooling after 50 s are shown in in Fig. 4. a), b) and c) for enameled iron, stainless steel, and aluminium respectively. In case of enameled iron the temperature decreased faster than the other two pots. In case of stainless steel the temperature was maintained after the induction cooker was switched off.

B. Temperature distribution of the pots

Fig. 5. a), c), e) shows the temperature distribution of the body side of the pots made of enameled iron, stainless steel and aluminum which have been observed during the heating process. It was observed that the enameled iron cookware reaches 250 °C in the area nearest to the base at 110 s then the temperature fluctuates around this value, whereas points from the central zone of its edge side increased the temperature linearly to 150 °C and the highest points of the lateral reached 100 °C. In the case of stainless steel, it need the double of time than the enameled iron to reach the same temperature, the highest point and the central points of the edge verified that the temperature is constant with values lower than 100 ° C, while the closest point of the base increased its temperature to 350 °C at 275 s, from there the temperature falls to 300 °C. In the case of aluminum pot, the behavior of the temperature in the middle and top points of the edge showed a similar behavior with a constant growth with values close to 50 °C at 200 s and then it decreased. In the case of the closest point to the base the temperature increased to 190 °C at 125 s, and then fluctuates.

The evolution of the temperature distribution of the side of the pots once the induction cooker was turned off, can be seen in Fig. 5. b), d), f). In the case of enameled iron is seen that the temperature of all points of the base decreased monotonically. In the case of the pots made of stainless steel and aluminum, the temperature behavior is similar in the central and top areas and it shows a monotonous decrease at first and then a decline steeper; in the case of the enameled iron body pot the temperature decreased from 225 °C to 100 °C in the first 50 s.

C. Heat flux distribution

The temperature distribution of the pots lateral, showed in Figure 3 was compared with the temperature distribution in the pots heated at 50 s, simulated by COMSOL Multiphysics© shown in Fig. 6. It is observed a correlation between the images obtained by the thermographic camera and the simulation.

From the temperature distribution simulated by COMSOL Multiphysics©, it was possible to calculate the heat flux from the pot.

In Figure 6 is observed the correlation between the heat flux and the temperature of the pan, even if a few measured points of heat flux were considered, just to confirm the accuracy of the distribution showed in Fig. 4 and validated by this way it was used as boundary conditions in case of IH.

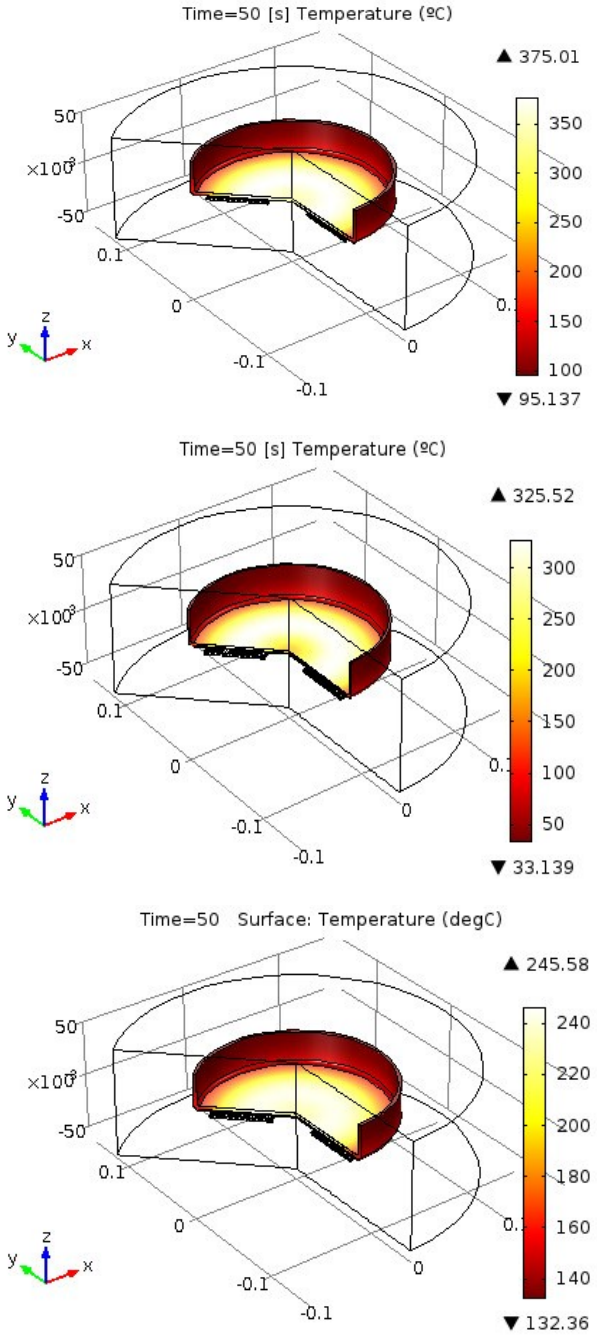

Fig. 6. Temperature distribution in the pot heated at 50 s, simulated by COMSOL a) enamelled iron, b) stainless steel and c) aluminium

The temperature and the heat flux in the pot were compared. The results under IH and GRH are shown in Fig. 5 a), b) and c), respectively. These figures revealed a correlation between the heat flux and the temperature of the pot, even a few measured points of heat flux were considered, just to confirm the accuracy of the distribution showed in Fig. 4 and validate by this way its use as boundary conditions in case of IH.

Results in Fig. 5 a) confirmed those showed in Fig. 4 a) in relation to the doughnut shape of the temperature profile of the bottom of the pan under IH when it has been increase the heating time. A similar behavior appears in Fig. 5 b) and c) at 45 s of the heating time.

D. Heat flux distribution in COMSOL

It has been performed an analysis of the heat flux from the pots bottom during heating process, from data of TABLE I and images shown in Fig. 4. It has been performed a simulation considering that the pots bottom receive a 1 000 W power in all of its surface. Fig. 9. Shows the results obtained from the heat flux of pots bottom at 15 s, 30 s y 50 s of the heating process. The convection heat fluxes are higher in the case of enameled iron, which is the one that reaches a higher temperatura in less time. While the pots made of stainless Steel and aluminium body present lower heat fluxes. It can be stated that the heat transfer is optimal. The results presented in Fig 6. a) confirmed that images showed in Fig. 5a)-c). The shape of circular ring of the temperature profile that is produced in the enameled iron pot, can be seen. In this case the process of heating of the pot bottom is similar to the one of the induction cooker coil, which usually has a diode in its central zone that turns off the cooker in case of registering very high temperatures. In the case of introducing a liter of water in the enamled iron pot, the temperatura distribution of the bottom is uniform.

In the case of stainless steel, Fig 6. b). shows results similar to the ones presented in 4 d)-f).; it can be seen that the heat flux increased in the bottom edge due to that the material thickness in the bottom edges is lower for this pot. In the case of the aluminium pot behavior, showed in Fig 6. c), it can be seen a higher heat flux in the central zone of the pot due to the configuration of the cookware design, in order to suit the zone that has more ferromagnetic material to the central zone of the pot.

CONCLUSIONS

In this investigation have been observed the heating rate is higher in iron enameled pots than the stainless steel or aluminum body cookware.

The multi analytic software COMSOL Multiphysics© validated the data obtained from a thermographic camera, through laboratory tests and recreate the same study. In this sense is thermographic camera is an interesting instrument for validate heat transfer analysis.

ACKNOWLEDGMENT

The authors of this present research acknowledge to the Secretaría Nacional de Planificación y Desarrollo (SENPLADES) for financing the execution of the present research. This work was sponsored by the Prometeo project of the Secretaria de Educación Superior, Ciencia, Tecnología e Innovación (SENESCYT) held in the Republic of Ecuador. The information necessary to complete this work was given by the Ministerio de Electricidad y Energía Renovable (MEER) of Ecuador.

REFERENCES

[1] A. Power, “Reducing the Number of Measurements in Induction Cooker Design,” no. 1, pp. 450–454, 2009.

[2] K. Frogner, M. Andersson, T. Cedell, L. Svensson, and P. Jeppsson, “induction technology.” pp. 215–223, 2003

[3] J. Schedel, I. Khan, and E. Uken, “Development of an induction cooker .,” pp. 73–78, 2002.

[4] B. Kos, B. Valič, D. Miklavčič, T. Kotnik, and P. Gajšek, “Pre- and post-natal exposure of children to EMF generated by domestic induction cookers.,” *Phys. Med. Biol.*, vol. 56, no. 19, pp. 6149–60, Oct. 2011.

[5] W. Arthur K.K. et al., “Experimental Study of Induction Cooker Fire Hazard,” *Procedia Eng.*, vol. 52, pp. 13–22, Jan. 2013.

[6] G. Cerri, S. a. Kovyryalov, V. Mariani Primiani, and P. Russo, “Rigorous Electromagnetic Analysis of Domestic Induction Heating Appliances,” *PIERS Online*, vol. 5, no. 5, pp. 491–495, 2009.

[7] H. W. Koertzent, J. D. Van Wyk, and J. A. Ferreira, “Design of the Half-Bridge, Series Resonant Converter for Induction Cooking,” pp. 1-24, 1995.

[8] H. Kawakami, Y. Llave, M. Fukuoka, and N. Sakai, “CFD analysis of the convection flow in the pan during induction heating and gas range heating,” *J. Food Eng.*, vol. 116, no. 3, pp. 726–736, Jun. 2013.

[9] Marco Orozco, Javier Martínez, Augusto Riofrío, Diego Vaca, Diego Carrión “Estudio de ensayos de eficiencia energética, concavidad, convexidad y rugosidad en menaje para cocinas de inducción” Memorias del Congreso latinoamericano de ingeniería mecánica Colim VIII, pp 255-261, 2014.

[10] Augusto Riofrío, Diego Vaca, Diego Carrión Marco Orozco, Javier Martínez, “Análisis del consumo energético en procesos de cocción eficiente para el sector residencial” Memorias del Congreso latinoamericano de ingeniería mecánica Colim VIII, pp 268-273, 2014.